# Cold-atom-based implementation of the quantum Rabi model

P. Schneeweiss,[1,][*] A. Dareau,[1] and C. Sayrin[1,2]

[1]*Vienna Center for Quantum Science and Technology, Atominstitut, TU Wien, Stadionallee 2, 1020 Vienna, Austria*
[2]*Laboratoire Kastler Brossel, Collège de France, CNRS, ENS-Université PSL, Sorbonne Université,*
*11 place Marcelin Berthelot, 75231 Paris Cedex 05, France*

The interaction of a two-level system (TLS) with a single bosonic mode (BM) is one of the most fundamental processes in quantum optics. Microscopically, it is described by the quantum Rabi model (QRM). Here we propose a versatile implementation of this model based on single trapped cold atoms. Assuming realistic experimental conditions, we show that our approach is not restricted to the Jaynes-Cummings regime but also allows exploring the regimes of ultrastrong coupling, deep strong coupling, and dispersive deep strong coupling. In contrast to most other QRM platforms, all important system parameters, i.e., the emitter-field detuning and the coupling strength of the emitter to the mode, can be dynamically tuned over a wide range. The quantum state of the BM and the TLS can be prepared and read-out using standard cold-atom techniques, enabling the study of the QRM and its dynamics with unprecedented control. Our scheme implements the TLS using atomic Zeeman states, while the atom's vibrational states in the trap represent the BM. The coupling is mediated by a suitable fictitious magnetic field pattern. Finally, we show that our scheme also enables the implementation of important generalizations, namely, the driven QRM, the QRM with quadratic coupling, or the Dicke model.

A two-level system (TLS) interacting with a single bosonic mode (BM) is described at the microscopic level by the quantum Rabi model (QRM) [1,2]. Among the iconic systems described by the QRM are single real or artificial atoms coupled to a mode of a resonator as well as single trapped ions. In the former case, the BM corresponds to microwave or optical photons while the TLS is realized by internal states of the atom. In the latter case, the quantized motion of the ion represents the BM. For the majority of experimental systems, the coupling strength is small, and the rotating-wave approximation can be applied, yielding the Jaynes-Cummings (JC) model. This is, arguably, one of the most successful theoretical frameworks in quantum optics [3,4].

Recently there has been a growing interest in the full QRM, which is valid for arbitrary ratios of the coupling strength $g$ and the mode frequency $\omega$. The Hamiltonian reads

$$\hat{H} = \hbar\omega\hat{a}^\dagger\hat{a} + \hbar g(\hat{a} + \hat{a}^\dagger)(\hat{\sigma}^+ + \hat{\sigma}^-) + \frac{\hbar\omega_0}{2}\hat{\sigma}_z, \quad (1)$$

with the bosonic creation (annihilation) operators $\hat{a}^\dagger$ ($\hat{a}$), the TLS's raising (lowering) operators $\hat{\sigma}^+$ ($\hat{\sigma}^-$), the Pauli matrix $\hat{\sigma}_z$, and the energy of the TLS $\omega_0$. Despite its fundamental nature, an analytic expression for the spectrum of the QRM was only found recently [5]. Remarkably, for large $g/\omega$, qualitatively new phenomena [6] such as the excitation of two atoms with one photon [7] are predicted and novel protocols for quantum information processing and quantum communication have been proposed [8–10]. A quantum phase transition, expected in the regime of large dispersive coupling, has attracted special interest, too [11].

The QRM in the regime where $g$ is a significant fraction of $\omega$ (ultrastrong coupling, USC) has been entered with several experimental systems including quantum wells [12–15], superconducting systems [16–18], and molecular ensembles [19,20]. Recently, ratios $g/\omega > 1$ were reached [21,22], corresponding to the deep-strong coupling (DSC) regime (see [23] for a detailed classification of coupling regimes). Despite this tremendous experimental progress, it is an open challenge to find fully versatile implementations of the QRM. Ideally, these allow for a flexible adjustment of the model parameters while providing ways to prepare and read-out the system's quantum state. Without these capabilities, a systematic study of the QRM dynamics is hampered. Alternatively, dedicated simulators have been proposed [24,25] and demonstrated [26,27], including approaches using ensembles of cold atoms [28,29].

Here we describe a way to directly implement the QRM using single trapped cold atoms in suitable magnetic field patterns. Our approach allows us to dynamically tune the system parameters ($g$, $\omega$, $\omega_0$) relative to each other over a wide range. Remarkably, assuming realistic experimental conditions, our scheme enables access to the USC and DSC and dispersive DSC (dDSC) regimes, the latter requiring $\omega_0 \gg g > \omega$ [29]. The initialization and read-out of the TLS's and the BM's states can be achieved using established cold-atom techniques [30]. These powerful means of control grant access to the study of dynamical properties of the QRM, including responses to adiabatic ramps or quenches. In the following we quantitatively discuss experimental parameters for the example of cold Rubidium atoms confined in a one-dimensional optical lattice. However, our approach can be implemented with any atom that has suitable polarizability properties and for which control over all degrees of freedom at the quantum level

---

[*]philipp.schneeweiss@tuwien.ac.at

is available, e.g., the other alkalis. Finally, we present the implementation of important generalizations of the QRM.

In order to introduce the underlying principle of our approach, we initially consider a canonical TLS, a spin-1/2 particle of mass $M$, confined along the $x$ direction in a one-dimensional harmonic trap of frequency $\omega$ and exposed to a tailored magnetic field. The Hamiltonian reads

$$\hat{H} = \hbar\omega\hat{a}^\dagger\hat{a} + g_L\mu_B \boldsymbol{B} \cdot \hat{\boldsymbol{S}}/\hbar, \tag{2}$$

with $\hat{\boldsymbol{S}} = (\hbar/2)\hat{\boldsymbol{\sigma}}$ and $\hat{\boldsymbol{\sigma}} = (\hat{\sigma}_x, \hat{\sigma}_y, \hat{\sigma}_z)$ the Pauli matrices, $\mu_B$ the Bohr magneton, and $g_L$ the Landé factor. The position-dependent magnetic field $\boldsymbol{B} = (b_x \hat{x}, 0, B_z)$ consists of a constant component along $z$ and a linearly varying $x$ component. While such a pattern cannot be implemented with real magnetic fields only ($\nabla \cdot \boldsymbol{B} = b_x \neq 0$), it can be realized by combining real and so-called fictitious magnetic fields, originating from the vector ac-Stark shift [31–33]. Fictitious magnetic fields can be obtained when a multilevel atom is exposed to a light field whose detuning is large compared the hyperfine splitting of the closest optical transition but not large compared to the fine-structure splitting. The induced magnetic field is maximal for circular polarization of the light and vanishes for linear polarization. Such fictitious fields can naturally arise in optical microtraps [34–36] and in certain optical lattice configurations [37–39]. Such lattices have, e.g., been used to implement degenerate Raman cooling [37,38], yet with many atoms per trapping site such that collisions can change the atom's spin and motional states in uncontrolled ways, with small coupling strength between the internal and external degrees of freedom, and/or in the incoherent regime due to scattering of trap and repumping light. The Hamiltonian that we consider here reads

$$\hat{H} = \hbar\omega\hat{a}^\dagger\hat{a} + g_L\mu_B/2\,(b_x\hat{x}\hat{\sigma}_x + B_z\hat{\sigma}_z). \tag{3}$$

We rewrite (3) using $\hat{x} = x_0(\hat{a} + \hat{a}^\dagger)$, with $x_0 = \sqrt{\hbar/(2M\omega)}$, and $\hat{\sigma}_x = \hat{\sigma}^+ + \hat{\sigma}^-$, which yields precisely the QRM Hamiltonian (1). Here the BM corresponds to motional states of the atom in the trap. The coupling strength and energy of the TLS are given by $g = (\mu_B g_L b_x x_0)/(2\hbar)$ and $\omega_0 = \mu_B g_L B_z/\hbar$, respectively.

We now discuss an implementation of Hamiltonian (3). We consider atoms of spin $F$ in their electronic ground state. We assume an optical lattice [40] resulting from the interference of two counterpropagating laser beams of wave number $k_t = 2\pi/\lambda_t$, linearly polarized along the same axis, see Fig. 1. We refer to this lattice as the *trapping lattice*. The induced trapping potential is proportional to the intensity of the resulting standing wave. We assume that each lattice site is occupied by, at most, one atom [41]. In order to induce a coupling between the spin and motional degrees of freedom, we consider another optical lattice, called the *coupling lattice*, consisting of two counterpropagating laser beams ($k_c = 2\pi/\lambda_c$) with orthogonal linear polarizations. The intensity of the combined field is uniform along the $x$ direction but the polarization changes with position. This gives rise to a spatially varying fictitious magnetic field $\boldsymbol{B}_{\text{fict}}(\hat{x}) = B_x \sin(2k_c\hat{x})\boldsymbol{e}_x$ [39], with $\boldsymbol{e}_x$ the unit vector along $x$. The total Hamiltonian, including the Zeeman shift due to an external homogeneous offset magnetic field

along the $z$ direction $B_z$ reads

$$\begin{aligned}
\hat{H} = {} & \frac{\hat{p}^2}{2M} + \frac{V_0}{2}(1 - \cos[2k_t\hat{x}]) \\
& + \frac{g_F\mu_B}{2}(B_x \sin[2k_c\hat{x}]\hat{F}_x + B_z\hat{F}_z), \tag{4}
\end{aligned}$$

with $V_0$ the trap depth, $\hat{F}_{x,y}$ the spin angular momentum operators, and $g_F$ the hyperfine Landé factor. The amplitude of the fictitious magnetic field $B_x$ is proportional to the intensity $I_c$ of the laser generating the coupling lattice. The wavelengths and the relative phase of the two lattices are chosen such that the local minima of the trapping sites coincide with the zero crossings of $\boldsymbol{B}_{\text{fict}}$. The trapping lattice is assumed to be sufficiently deep, such that tunneling between neighboring sites can be neglected [42]. Near the local minima, the trapping potential is approximated by an harmonic potential with an effective frequency $\omega_{\text{eff}} \approx 2\sqrt{V_0 E_r}/\hbar$ where $E_r = \hbar^2 k_t^2/(2M)$ is the recoil energy. Around these minima, the fictitious field is well approximated by a linear gradient $\boldsymbol{B}_{\text{fict}} \approx b_x\hat{x}\boldsymbol{e}_x$, with $b_x \approx 2B_x k_c$. The corresponding effective coupling strength is then given by $g_{\text{eff}} \approx (\mu_B g_L B_x k_c x_0)/\hbar$. We then obtain an array of trapping sites, where each site realizes the QRM Hamiltonian (1), whose parameters can be widely tuned: The coupling strength can be adjusted, independently from other parameters, by tuning the intensity $I_c$ of the coupling lattice ($g_{\text{eff}} \propto I_c$). The mode frequency $\omega_{\text{eff}}$ can be adjusted via the trap depth ($\omega_{\text{eff}} \propto \sqrt{V_0}$), which also changes $g_{\text{eff}}$ via $x_0 \propto V_0^{-1/4}$. The energy of the TLS $\omega_0$ can be adjusted independently via $B_z$ ($\omega_0 \propto B_z$). The tuning methods available for our approach are very versatile and allow us to modulate all parameters in tenths or hundredths of the system's intrinsic timescale. These modulation capabilities are of interest to study nonadiabatic phenomena of the QRM such as the dynamical Casimir effect [43]. As quantitatively discussed in the following, our approach does not only allow us to explore the JC regime but also the regimes of USC, DSC, or dDSC.

We now consider the case of the commonly used isotope of Rubidium, $^{87}$Rb. A large fictitious magnetic field can be obtained when $\lambda_c$ is close to the Rubidium $D_1$ and $D_2$ lines (see, e.g., Ref. [44] for an in-depth discussion of light shifts for $^{87}$Rb). A simple choice for $\lambda_t$ is $\lambda_t = \lambda_c$. In this case, both lattices can be generated with a single pair of counterpropagating beams with linear polarizations tilted with respect to each other by an angle $\theta$ ("lin-$\theta$-lin" configuration), see Fig. 1. The relative strength of the coupling and trapping lattices, and, thus, the ratio $g_{\text{eff}}/\omega_{\text{eff}}$, can be tuned by varying $\theta$. One can also use independent light fields to generate the coupling and trapping lattices. In this case, the relative phase of the two lattices needs to be stabilized. An interesting choice for $\lambda_c$ is then the tune-out wavelength (790.0 nm for Rb) [45], where the atom's scalar polarizability vanishes, so that the coupling lattice only induces a fictitious magnetic field. The matching of the local trap minima with the magnetic field zero crossings can be ensured by choosing, for instance, $\lambda_t = 2\lambda_c$ or $\lambda_t = (3/2)\lambda_c$. In the second case, the sign of $g_{\text{eff}}$ alternates from site to site.

A set of realistic parameters for the two configurations is presented in Table I. Remarkably, we obtain $g_{\text{eff}}/\omega_{\text{eff}} \approx 3$, i.e., clearly in the DSC regime. The external magnetic field $B_z$
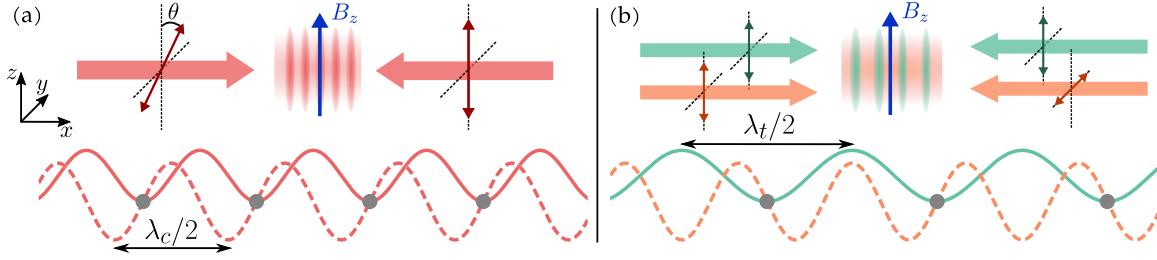
FIG. 1. Sketch of the experimental implementation for the two proposed configurations. The propagation directions of the light fields are indicated by single-sided arrows, their (linear) polarizations are indicated by double-sided arrows. The blue arrow indicates the external homogeneous magnetic field. The trapping potential (solid line) and the fictitious magnetic field (dashed line) are also shown. The atoms' positions are marked with gray dots. Each trapping site realizes an implementation of the QRM Hamiltonian. (a) Lin-$\theta$-lin lattice ($\lambda_c = \lambda_t$). (b) Two-lattices configuration [$\lambda_t = (3/2)\lambda_c$].

allows a flexible choice of $\omega_0$. For instance, in the case of Table I(a), $\omega_0 = \omega_{\text{eff}}$ corresponds to $B_z \approx 4\,\text{G}$. The trapping (coupling) lattice light field is inelastically scattered by the atoms with the rate $\Gamma_t \propto I_t$ ($\Gamma_c \propto I_c$). The ratio $g_{\text{eff}}/\Gamma_c$ is a constant. We estimate that $\Gamma_t$ and $\Gamma_c$ are orders of magnitude smaller than $g_{\text{eff}}$. Inelastic scattering is thus negligible during many cycles of coherent evolution. Other sources of decoherence include heating of the atoms or magnetic field noise. In typical optical-lattice setups, decoherence rates of less than 10 Hz can be obtained [46]. Given these values, both effects should be irrelevant on the timescales considered here.

Deviations from the harmonic approximation are expected for large energies: The wave functions and energies of highly excited states in the trapping lattice differ from those of the harmonic oscillator. Moreover, the fictitious magnetic field is well approximated by a linear gradient only close to the field zero crossings. In order to quantify these effects, we perform a numerical diagonalization of Hamiltonian (4) in position-spin space [47], and compare the obtained eigenenergies and eigenfunctions with the ones of the QRM. For this comparison we have to chose effective values $g_{\text{eff}}$ and $\omega_{\text{eff}}$ as introduced when mapping Hamiltonian (4) to Hamiltonian (1). These effective values, which can differ from the ones extracted from a series expansion of (4), are obtained as follows. When setting $B_z = 0$, the Hamiltonian (4) is diagonal in the $\hat{F}_x$ basis.

TABLE I. Example parameters for implementing the QRM with $^{87}$Rb for effective coupling strength $g_{\text{eff}}$ and mode frequency $\omega_{\text{eff}}$. In (a) we indicate the power $P$ per laser beam and the relative angle $\theta$ between their linear polarizations. In (b) $P_t$ ($P_c$) is the power per trapping (coupling) lattice laser beam. Rates $\Gamma_t$ and $\Gamma_c$ ($\Gamma = \Gamma_t + \Gamma_c$) quantify inelastic scattering. Lattice laser beam waists: $w = 15\,\mu$m.

| Parameter | (a) Lin-$\theta$-lin | (b) Two lattices | Unit |
|---|---|---|---|
| $\lambda_t$ | 787 | 1185 | nm |
| $\lambda_c$ | | 790.04 | nm |
| Specific | $P = 2.6$ W | $P_t = 14$ W | – |
| configuration | $\theta \approx 49°$ | $P_c = 0.75$ W | – |
| $V_0$ | $1 \times 10^5$ | $2 \times 10^5$ | $E_r$ |
| $\omega_{\text{eff}}/(2\pi)$ | 2.9 | 2.2 | MHz |
| $g_{\text{eff}}/(2\pi)$ | 8.5 | 6.5 | MHz |
| Scattering | $\Gamma = 16.9$ | $\Gamma_t = 0.09$ | kHz |
| rate | | $\Gamma_c = 3.6$ | kHz |

We then fit the effective potential for the high-field seeking Zeeman substate near its local minimum. The local curvature then determines $\omega_{\text{eff}}$ while the position of the minimum yields $g_{\text{eff}}$. The discrepancy between the $g_{\text{eff}}/\omega_{\text{eff}}$ ratio obtained using this method and the one derived from the analytical series expansion of (4) increases for larger values of the coupling strength, but is at most about 10%. Note that this quantity is not a measure for the quality of the QRM implementation: the latter is only given by $\overline{\Delta E}$ and $\overline{\mathcal{I}}$ as shown in Fig. 2.

The results of a systematic comparison between the QRM and our implementation are summarized in Fig. 2, accounting for several trapping lattice depths and $0 \leqslant g_{\text{eff}}/\omega_{\text{eff}} \leqslant 3$. For every configuration we compare the first 30 eigenstates, corresponding to the first 10 motional states for $^{87}$Rb in the $F = 1$ hyperfine state. For the parameters of Table I, the mean agreement of the eigenenergies is better than 1% and 2% for the "lin-$\theta$-lin" and the "two-lattices" configuration, respectively. This holds for all considered $g_{\text{eff}}/\omega_{\text{eff}}$ values. The mean infidelity of the eigenfunctions is less than $2 \times 10^{-3}$ and $10^{-1}$, respectively. The results are essentially unchanged when varying $\omega_0$.

A simple experimental test of the system consists in inducing the familiar Rabi oscillations encountered in the JC regime. For this purpose, a single atom is initialized in the motional ground state using standard techniques [30]. An offset magnetic field is applied and the atom is optically pumped into an energetically higher-lying Zeeman substate, i.e., an eigenstate of the QRM Hamiltonian for $g_{\text{eff}} = 0$. In order to start the Rabi oscillations, $g_{\text{eff}}$ is switched on abruptly by rapidly ramping up the coupling lattice. Then the atomic population oscillates between the different internal states until the coupling is switched off again. The state population can then be measured by, e.g., state-selective optical read-out. A full tomography of the internal state of the atom can be performed, for example, using Raman adiabatic passage techniques [48–50] or dispersive optical probing [51]. The occupation of the BM, corresponding to the population of the motional states of the trap, can also be obtained using standard cold-atoms techniques [34,35,52,53]. Repeating this experiment with larger $g_{\text{eff}}/\omega_{\text{eff}}$ ratios and different detunings then allows the study of genuine QRM effects [6,54]. Although there has been impressive progress on the experimental study of the QRM, most experiments are, so far, limited to spectroscopic analyses. Dynamics signatures have been measured for $g/\omega \approx 0.1$ [15], and the dynamics for larger coupling has been
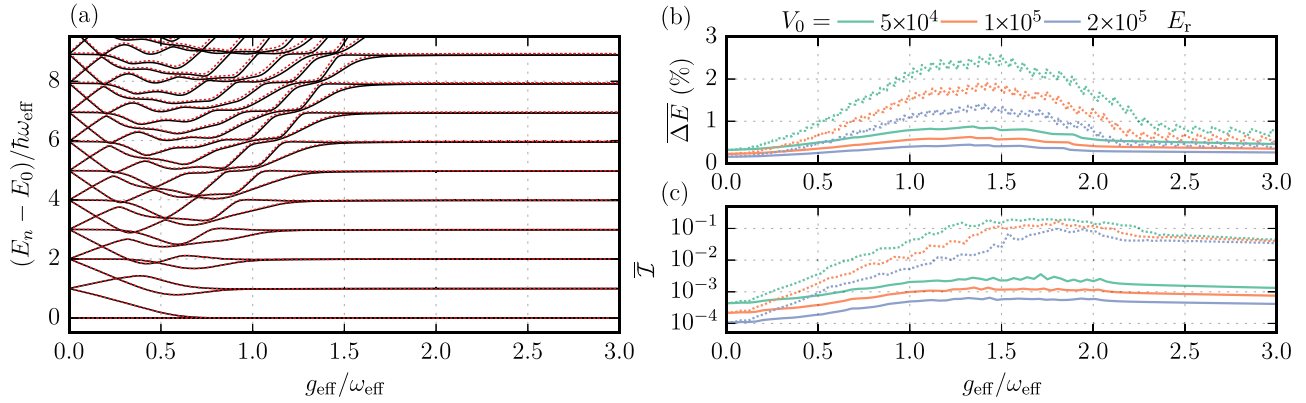
FIG. 2. Comparison between the ideal QRM (index "th") and our implementation (index "expt") for the first 30 eigensolutions $\{E_n, |\psi_n\rangle\}$ as a function of $g_{\text{eff}}/\omega_{\text{eff}}$. (a) Energies $E_n^{\text{th}}$ (red dashed lines) and $E_n^{\text{expt}}$ for "lin-$\theta$-lin" implementation (solid black lines). Parameters as in Table I(a). (b) Mean energy discrepancy $\overline{\Delta E} = (1/N) \sum_{n<N} |1 - E_n^{\text{expt}}/E_n^{\text{th}}|$. Solid lines: lin-$\theta$-lin configuration, dashed lines: "two-lattices" configuration. Different colors correspond to different depths $V_0$ of the trapping lattice: green (top), orange (middle), and blue (bottom) lines correspond to a depth of $5 \times 10^4 E_r$, $1 \times 10^5 E_r$, and $2 \times 10^5 E_r$, respectively, and $E_r$ denoting the recoil energy. All calculations are done on resonance, $\omega = \omega_0$. (c) Mean state infidelity $\overline{\mathcal{I}} = (1/N) \sum_{n<N} 1 - |\langle \psi_n^{\text{th}} | \psi_n^{\text{expt}} \rangle|^2$. The maximum discrepancies for our optimum setting are about 3% and 1% for the eigenenergies and eigenfunctions, respectively.

observed in a digital quantum simulation [55]. Our approach gives access to the QRM dynamics and should, for example, facilitate the direct observation of the collapse and revival predicted in the DSC regime [6]. Another option enabled by our *in situ* control of the parameters is the adiabatic preparation of the ground state of the QRM, which exhibits entanglement between the BM and the TLS [23]. These examples emphasize the new opportunities created by our approach.

Our scheme can be adapted to implement important variations of the QRM [56]. For example, in addition to $B_z$, one can introduce a constant component $\epsilon$ along $x$. The total magnetic field is then $\boldsymbol{B} = (b_x \hat{x} + \epsilon, 0, B_z)$, which yields an additional term $g_\epsilon \hat{F}_x$ with $g_\epsilon = \epsilon \mu_B g_F/2$ in (4), realizing the driven Rabi model. One of many interesting phenomena predicted for this system is the emergence of Dirac conelike intersections in the system's energy landscape [57]. This setting reduces to the well-known state-dependent optical lattice [39] for $B_z = 0$.

So far we overlapped the zero crossings of the coupling lattice with the minima of the trapping lattice. Another option is to spatially match the local extrema of both lattices. Then the atoms are exposed to a curved magnetic field $B_x \approx B_x^{(0)} + b_{xx} \hat{x}^2$. This yields a coupling $\hbar g_2 (\hat{a} + \hat{a}^\dagger)^2 \hat{F}_x$ with $g_2 = \mu_B g_F b_{xx} x_0^2/(2\hbar)$. Note that the series expansion of the fictitious magnetic field, in addition to the quadratic term, leads to an homogeneous component pointing along $x$, $B_x^{(0)}$. Such a component is present in the case of the driven QRM, and can be easily compensated if required. For quadratic coupling, the emergence of darklike states [58] has been predicted. Moreover, a spectral collapse [59,60], where all eigenenergies of the system approach a common value, is among the most remarkable effects of this model. Our approach should allow the study of quadratic coupling. Tunneling between lattice sites, however, might have to be taken into account for large $g_2$ as it leads to a reduction of the effective trap depth.

Until now we have considered an implementation using $^{87}$Rb in its $F = 1$ spin state while the QRM considers a TLS. A spin-1/2 is encountered in the lower hyperfine ground state of $^6$Li. Lithium is commonly used in cold-atom exper-

iments, and its ground-state cooling has been demonstrated [61]. However, heavier alkali atoms offer easier laser cooling and imaging. Moreover, they feature large fine-structure splittings which offer a more favorable ratio $|\boldsymbol{B}_{\text{fict}}|/\Gamma_c$ when implementing fictitious magnetic fields via a tune-out light field. Different means have been developed to constrain a system to a sub-Hilbert space [62]. For example, using Raman coupling, the coherent evolution of Rabi oscillations between the five Zeeman substates in $^{87}$Rb, $F = 2$ has been restricted to $|F = 2, m_F = 1\rangle$ and $|F = 2, m_F = 2\rangle$, effectively realizing a spin-1/2 [63]. In this way, the QRM can be implemented while benefiting from the advantages of heavier alkalis. Note that for the implementation of the QRM, either via a natural spin-1/2 or by constraining the Hilbert space, tensorial light shifts are irrelevant.

Working with large spins is of interest on its own as it enables the experimental study of the Dicke model, describing $N$ identical spin-1/2 coupled to a common mode. The Hamiltonian reads

$$\frac{\hat{H}_D}{\hbar} = \omega \hat{a}^\dagger \hat{a} + \frac{\omega_0}{2} \sum_{i=1}^{N} \hat{\sigma}_z^{(i)} + \frac{g}{\sqrt{N}} (\hat{a} + \hat{a}^\dagger) \sum_{i=1}^{N} \hat{\sigma}_x^{(i)}. \quad (5)$$

We introduce $\hat{F}_{\alpha=\{x,z\}} = 1/2 \sum_i \hat{\sigma}_\alpha^{(i)}$ the angular momentum operators of a pseudo-spin-$N/2$. Since a unitary evolution with Hamiltonian (5) preserves $F$, a single spin-$F$ particle equivalently represents the Dicke model with $N = 2F$ particles in the subspace spanned by the states $|F, m_F = -F \cdots F\rangle$. Therefore, $^{87}$Rb in the state $F = 2$ allows one to simulate the Dicke model for $N = 4$. The isotope $^{85}$Rb, which can be cooled and trapped with the same lasers, allows for the simulation of $N = 6$ when prepared in $F = 3$. Note that, in contrast to the QRM case, our implementation of the Dicke model might, in principle, be affected by tensorial light shifts. These would lead to an anharmonicity in the energy spacing of the $N$-level system. However, for the cases discussed in Table I, the tensorial shift is about a factor of $10^{-5}$ and $10^{-4}$ smaller than the vectorial light shift for the cases (a) and (b), respectively. The tensor light shift

for the considered settings is much smaller than all other terms in the Hamiltonian (4) and, thus, completely negligible. The Dicke model features a quantum phase transition, expected to occur at large enough coupling strength [64]. It has been shown that signatures of this transition prevail for a finite-size system constrained to the largest pseudospin subspace [64], such that it might be observable with our approach. More generally, our scheme might enable extending the very successful experimental studies of the Dicke model that rely on large atomic ensembles in cavities [65] to the mesoscopic regime.

In summary, we propose a cold-atom-based platform for the experimental investigation of the QRM including its dynamics. Remarkably, assuming realistic experimental conditions, our estimations predict that the implementation of the QRM in the USC, DSC, and dDSC regime should be feasible. Corresponding experiments can take advantage of the rich toolbox developed in cold-atom physics, facilitating state preparation and read-out of the system. Moreover, we have presented ways to implement important generalizations of the model.

Future theory work might conceive extensions of our scheme to further generalizations. For example, effective spin-spin interactions in the Dicke model [66,67] might be introduced by an additional light field giving rise to a tensorial ac-Stark shift [32], yielding a $\hat{F}_x^2$ coupling. Moreover, our approach should allow USC of two BMs, and enable studying the Jahn-Teller instability with cold atoms [68,69]. Finally, the QRM in the presence of dissipation exhibits surprising, nontrivial effects [43]. Our approach might open up novel ways to their study and provide means to develop tools for quantum reservoir engineering [70] in the USC and DSC regimes.

[1] I. Rabi, Phys. Rev. **49**, 324 (1936).

[2] I. Rabi, Phys. Rev. **51**, 652 (1937).

[3] S. Haroche, Rev. Mod. Phys. **85**, 1083 (2013).

[4] D. J. Wineland, Rev. Mod. Phys. **85**, 1103 (2013).

[5] D. Braak, Phys. Rev. Lett. **107**, 100401 (2011).

[6] J. Casanova, G. Romero, I. Lizuain, J. J. García-Ripoll, and E. Solano, Phys. Rev. Lett. **105**, 263603 (2010).

[7] L. Garziano, V. Macrì, R. Stassi, O. Di Stefano, F. Nori, and S. Savasta, Phys. Rev. Lett. **117**, 043601 (2016).

[8] P. Nataf and C. Ciuti, Phys. Rev. Lett. **107**, 190402 (2011).

[9] G. Romero, D. Ballester, Y. M. Wang, V. Scarani, and E. Solano, Phys. Rev. Lett. **108**, 120501 (2012).

[10] T. H. Kyaw, S. Felicetti, G. Romero, E. Solano, and L.-C. Kwek, Sci. Rep. **5**, 8621 (2015).

[11] M.-J. Hwang, R. Puebla, and M. B. Plenio, Phys. Rev. Lett. **115**, 180404 (2015).

[12] A. A. Anappara, S. De Liberato, A. Tredicucci, C. Ciuti, G. Biasiol, L. Sorba, and F. Beltram, Phys. Rev. B **79**, 201303 (2009).

[13] G. Günter, A. A. Anappara, J. Hees, A. Sell, G. Biasiol, L. Sorba, S. De Liberato, C. Ciuti, A. Tredicucci, A. Leitenstorfer *et al.*, Nature (London) **458**, 178 (2009).

[14] Y. Todorov, A. M. Andrews, R. Colombelli, S. De Liberato, C. Ciuti, P. Klang, G. Strasser, and C. Sirtori, Phys. Rev. Lett. **105**, 196402 (2010).

[15] Q. Zhang, M. Lou, X. Li, J. L. Reno, W. Pan, J. D. Watson, M. J. Manfra, and J. Kono, Nat. Phys. **12**, 1005 (2016).

[16] J. Bourassa, J. M. Gambetta, A. A. Abdumalikov, O. Astafiev, Y. Nakamura, and A. Blais, Phys. Rev. A **80**, 032109 (2009).

[17] T. Niemczyk, F. Deppe, H. Huebl, E. Menzel, F. Hocke, M. Schwarz, J. Garcia-Ripoll, D. Zueco, T. Hümmer, E. Solano *et al.*, Nat. Phys. **6**, 772 (2010).

[18] P. Forn-Díaz, J. Lisenfeld, D. Marcos, J. J. García-Ripoll, E. Solano, C. J. P. M. Harmans, and J. E. Mooij, Phys. Rev. Lett. **105**, 237001 (2010).

[19] T. Schwartz, J. A. Hutchison, C. Genet, and T. W. Ebbesen, Phys. Rev. Lett. **106**, 196405 (2011).

[20] J. George, T. Chervy, A. Shalabney, E. Devaux, H. Hiura, C. Genet, and T. W. Ebbesen, Phys. Rev. Lett. **117**, 153601 (2016).

[21] F. Yoshihara, T. Fuse, S. Ashhab, K. Kakuyanagi, S. Saito, and K. Semba, Nat. Phys. **13**, 44 (2017).

[22] P. Forn-Díaz, J. García-Ripoll, B. Peropadre, J.-L. Orgiazzi, M. Yurtalan, R. Belyansky, C. Wilson, and A. Lupascu, Nat. Phys. **13**, 39 (2017).

[23] D. Z. Rossatto, C. J. Villas-Bôas, M. Sanz, and E. Solano, Phys. Rev. A **96**, 013849 (2017).

[24] J. Pedernales, I. Lizuain, S. Felicetti, G. Romero, L. Lamata, and E. Solano, Sci. Rep. **5**, 15472 (2015).

[25] R. Puebla, M.-J. Hwang, J. Casanova, and M. B. Plenio, Phys. Rev. Lett. **118**, 073001 (2017).

[26] J. Braumüller, M. Marthaler, A. Schneider, A. Stehli, H. Rotzinger, M. Weides, and A. V. Ustinov, Nat. Commun. **8**, 779 (2017).

[27] D. Lv, S. An, Z. Liu, J.-N. Zhang, J. S. Pedernales, L. Lamata, E. Solano, and K. Kim, Phys. Rev. X **8**, 021027 (2018).

[28] A. L. Grimsmo and S. Parkins, Phys. Rev. A **87**, 033814 (2013).

[29] S. Felicetti, E. Rico, C. Sabin, T. Ockenfels, J. Koch, M. Leder, C. Grossert, M. Weitz, and E. Solano, Phys. Rev. A **95**, 013827 (2017).

[30] C. Cohen-Tannoudji and D. Guéry-Odelin, *Advances in Atomic Physics: An Overview* (World Scientific, Singapore, 2011).

[31] C. Cohen-Tannoudji and J. Dupont-Roc, Phys. Rev. A **5**, 968 (1972).

[32] I. H. Deutsch and P. S. Jessen, Opt. Commun. **283**, 681 (2010).

[33] F. Le Kien, P. Schneeweiss, and A. Rauschenbeutel, Eur. Phys. J. D **67**, 92 (2013).

[34] A. M. Kaufman, B. J. Lester, and C. A. Regal, Phys. Rev. X **2**, 041014 (2012).

[35] J. D. Thompson, T. G. Tiecke, A. S. Zibrov, V. Vuletić, and M. D. Lukin, Phys. Rev. Lett. **110**, 133001 (2013).

[36] B. Albrecht, Y. Meng, C. Clausen, A. Dareau, P. Schneeweiss, and A. Rauschenbeutel, Phys. Rev. A **94**, 061401 (2016).

[37] S. E. Hamann, D. L. Haycock, G. Klose, P. H. Pax, I. H. Deutsch, and P. S. Jessen, Phys. Rev. Lett. **80**, 4149 (1998).

[38] V. Vuletić, C. Chin, A. J. Kerman, and S. Chu, Phys. Rev. Lett. **81**, 5768 (1998).

[39] O. Mandel, M. Greiner, A. Widera, T. Rom, T. W. Hänsch, and I. Bloch, Phys. Rev. Lett. **91**, 010407 (2003).

[40] R. Grimm, M. Weidemuller, and Y. B. Ovchinnikov, Adv. At. Mol. Opt. Phys. **42**, 95 (2000).

[41] N. Schlosser, G. Reymond, and P. Grangier, Phys. Rev. Lett. **89**, 023005 (2002).

[42] I. Bloch, J. Dalibard, and W. Zwerger, Rev. Mod. Phys. **80**, 885 (2008).

[43] F. Beaudoin, J. M. Gambetta, and A. Blais, Phys. Rev. A **84**, 043832 (2011).

[44] Q.-Q. Hu, C. Freier, Y. Sun, B. Leykauf, V. Schkolnik, J. Yang, M. Krutzik, and A. Peters, Phys. Rev. A **97**, 013424 (2018).

[45] B. Arora, M. S. Safronova, and C. W. Clark, Phys. Rev. A **84**, 043401 (2011).

[46] C. Robens, S. Brakhane, W. Alt, D. Meschede, J. Zopes, and A. Alberti, Phys. Rev. Appl. **9**, 034016 (2018).

[47] J. Johansson, P. Nation, and F. Nori, Comput. Phys. Commun. **183**, 1760 (2012).

[48] F. Vewinger, M. Heinz, R. Garcia Fernandez, N. V. Vitanov, and K. Bergmann, Phys. Rev. Lett. **91**, 213001 (2003).

[49] J. Volz, M. Weber, D. Schlenk, W. Rosenfeld, J. Vrana, K. Saucke, C. Kurtsiefer, and H. Weinfurter, Phys. Rev. Lett. **96**, 030404 (2006).

[50] F. Vewinger, M. Heinz, U. Schneider, C. Barthel, and K. Bergmann, Phys. Rev. A **75**, 043407 (2007).

[51] A. Smith, C. A. Riofrío, B. E. Anderson, H. Sosa-Martinez, I. H. Deutsch, and P. S. Jessen, Phys. Rev. A **87**, 030102 (2013).

[52] M. Morinaga, I. Bouchoule, J.-C. Karam, and C. Salomon, Phys. Rev. Lett. **83**, 4037 (1999).

[53] N. Belmechri, L. Förster, W. Alt, A. Widera, D. Meschede, and A. Alberti, J. Phys. B: At. Mol. Opt. Phys. **46**, 104006 (2013).

[54] F. A. Wolf, F. Vallone, G. Romero, M. Kollar, E. Solano, and D. Braak, Phys. Rev. A **87**, 023835 (2013).

[55] N. Langford, R. Sagastizabal, M. Kounalakis, C. Dickel, A. Bruno, F. Luthi, D. Thoen, A. Endo, and L. DiCarlo, Nat. Commun. **8**, 1715 (2017).

[56] D. Braak, Q.-H. Chen, M. T. Batchelor, and E. Solano, J. Phys. A: Math. Theor. **49**, 300301 (2016).

[57] M. T. Batchelor, Z.-M. Li, and H.-Q. Zhou, J. Phys. A: Math. Theor. **49**, 01LT01 (2016).

[58] J. Peng, C. Zheng, G. Guo, X. Guo, X. Zhang, C. Deng, G. Ju, Z. Ren, L. Lamata, and E. Solano, J. Phys. A: Math. Theor. **50**, 174003 (2017).

[59] K. Ng, C. Lo, and K. Liu, Eur. Phys. J. D **6**, 119 (1999).

[60] C. Emary and R. Bishop, J. Phys. A: Math. Gen. **35**, 8231 (2002).

[61] A. Omran, M. Boll, T. A. Hilker, K. Kleinlein, G. Salomon, I. Bloch, and C. Gross, Phys. Rev. Lett. **115**, 263001 (2015).

[62] J. M. Raimond, C. Sayrin, S. Gleyzes, I. Dotsenko, M. Brune, S. Haroche, P. Facchi, and S. Pascazio, Phys. Rev. Lett. **105**, 213601 (2010).

[63] F. Schäfer, I. Herrera, S. Cherukattil, C. Lovecchio, F. S. Cataliotti, F. Caruso, and A. Smerzi, Nat. Commun. **5**, 3194 (2014).

[64] C. Emary and T. Brandes, Phys. Rev. Lett. **90**, 044101 (2003).

[65] F. Dimer, B. Estienne, A. S. Parkins, and H. J. Carmichael, Phys. Rev. A **75**, 013804 (2007).

[66] T. Jaako, Z.-L. Xiang, J. J. Garcia-Ripoll, and P. Rabl, Phys. Rev. A **94**, 033850 (2016).

[67] D. De Bernardis, T. Jaako, and P. Rabl, Phys. Rev. A **97**, 043820 (2018).

[68] J. Larson, Phys. Rev. A **78**, 033833 (2008).

[69] C. P. Meaney, T. Duty, R. H. McKenzie, and G. J. Milburn, Phys. Rev. A **81**, 043805 (2010).

[70] J. F. Poyatos, J. I. Cirac, and P. Zoller, Phys. Rev. Lett. **77**, 4728 (1996).